Anisotropy of Solar-Wind Turbulence in the Inner Heliosphere at Kinetic Scales: PSP Observations

Die Duan,[1] Jiansen He,[1] Trevor A. Bowen,[2] Lloyd D. Woodham,[3] Tieyan Wang,[4] Christopher H. K. Chen,[5] Alfred Mallet,[2] and Stuart D. Bale[2, 6, 3, 5]

[1]*School of Earth and Space Sciences, Peking University, Beijing, 100871, China*
[2]*Space Sciences Laboratory, University of California, Berkeley, CA 94720-7450, USA*
[3]*The Blackett Laboratory, Imperial College London, London, SW7 2AZ, UK*
[4]*RAL Space, Rutherford Appleton Laboratory, Harwell Oxford, Didcot OX11 0QX, UK*
[5]*School of Physics and Astronomy, Queen Mary University of London, London E1 4NS, UK*
[6]*Physics Department, University of California, Berkeley, CA 94720-7300, USA*

ABSTRACT

The anisotropy of solar wind turbulence is a critical issue in understanding the physics of energy transfer between scales and energy conversion between fields and particles in the heliosphere. Using the measurement of *Parker Solar Probe* (*PSP*), we present an observation of the anisotropy at kinetic scales in the slow, Alfvénic, solar wind in the inner heliosphere. A steepened transition range is found between the inertial and kinetic ranges at all the directions with respect to the local background magnetic field direction. The anisotropy of $k_\perp \gg k_\parallel$ is found evident in both transition and kinetic ranges, with the power anisotropy $P_\perp/P_\parallel > 10$ in the kinetic range leading over that in the transition range and being stronger than that at 1 au. The spectral index varies from $\alpha_{t\parallel} = -5.7 \pm 1.3$ to $\alpha_{t\perp} = -3.7 \pm 0.3$ in the transition range and $\alpha_{k\parallel} = -2.9 \pm 0.2$ to $\alpha_{k\perp} = -2.57 \pm 0.07$ in the kinetic range. The corresponding wavevector anisotropy has the scaling of $k_\parallel \sim k_\perp^{2/3}$ in the transition range, and changes to $k_\parallel \sim k_\perp^{1/3}$ in the kinetic range, consistent with the kinetic Alfvénic turbulence at sub-ion scales.

Keywords: Space plasmas(1544) — Solar wind(1534) — Interplanetary turbulence(830)

1. INTRODUCTION

Magnetic field fluctuations in the solar wind are highly turbulent. The measured power spectral density (PSD) of fluctuating magnetic field always exhibits power laws $k^{-\alpha}$, where k is the wavenumber, and α is the spectral index. A single spacecraft measures the PSD as a function of $f^{-\alpha}$ in the frequency domain, which can be converted to the spatial domain under the Taylor Hypothesis. According to the physical processes at different scales, the PSD in the solar wind can be divided into several segments, which can be fitted with different α. The inertial range, which is dominated by magnetohydrodynamic (MHD) turbulence, follows the cascade models with spectral indices α_i from around 3/2 to 5/3 (Bruno & Carbone 2013; Chen et al. 2020). The PSDs become steepened below the ion scales (ion thermal gy-

roradius ρ_i or ion inertial length d_i), where kinetic mechanisms should be taken into account. Sometimes a sharp transition range is observed with $\alpha_t \sim 4$ (Sahraoui et al. 2010; Bowen et al. 2020a). This transition range may be caused by imbalanced turbulence (Voitenko & Keyser 2016; Meyrand et al. 2020) (Woodham et al. 2021, in perp.), energy dissipation of kinetic waves (Howes et al. 2008), ion-scale coherent structures (Lion et al. 2016), or a reconnection dominated range (Mallet et al. 2017). At smaller scales, a flatter sub-ion kinetic range forms with the spectral index $\alpha_k \sim 7/3$, which can be explained as the MHD Alfvénic turbulence developing into a type of kinetic wave turbulence, e.g., kinetic Alfvén waves (Bale et al. 2005; Chen et al. 2013) or whistler waves (Saito et al. 2008). Intermittency in the kinetic range could lead to an 8/3 spectrum (Boldyrev & Perez 2012; Zhao et al. 2016). The spectral indices increase again beyond the electron kinetic scales, indicating the turbulence energy dissipates to electrons (Sahraoui et al. 2009;

Alexandrova et al. 2012; Chen et al. 2019) or transitions to a further dispersive cascade (Chen & Boldyrev 2017).

Because of the background interplanetary magnetic field (IMF), the turbulence in the solar wind is anisotropic. At the MHD scales, the energy transfer rate depends on the angle θ_{kB} between the wavevector $\mathbf{k}$ of fluctuations and the background magnetic field (Goldreich & Sridhar 1995). The anisotropic energy cascade could lead to the anisotropy of power level and spectral index (Chen et al. 2010b), which is observed in the solar wind turbulence (Horbury et al. 2008; Podesta 2009). Goldreich & Sridhar (1995) also predicts a critical balanced wavevector anisotropy of $k_\parallel \sim k_\perp^{2/3}$ and Boldyrev (2006) predicts $k_\parallel \sim k_\perp^{1/2}$. Here $k_\perp$ is the wavevector perpendicular to the background magnetic field direction, and $k_\parallel$ is the wavevector along the parallel direction. He et al. (2013) found that turbulent power is enhanced along a ridge at $k_\perp > k_\parallel$ in the 2D wavevector space. Moreover, it is argued that other possible reasons could lead to the observed anisotropy, such as intermittency (Wang et al. 2014), solar wind expansion (Verdini et al. 2019) and non-stationarity of the background magnetic field (Wu et al. 2020). How the MHD-scale anisotropy rises in the solar wind is still a challenging question.

In the kinetic range, the fluctuations remain anisotropic. Theoretically, the specific form of wavevector anisotropy will depend on the nature of the fluctuations. The kinetic Alfvénic wave (KAW) turbulence models predict $k_\parallel \sim k_\perp^{1/3}$ (Howes et al. 2008; Schekochihin et al. 2009). The intermittent KAW model gives the scaling of $k_\parallel \sim k_\perp^{2/3}$ (Boldyrev & Perez 2012). The tearing-instability-mediated-turbulence model predicts from $k_\parallel \lesssim k_\perp^{2/3}$ to $k_\parallel \lesssim k_\perp$ (Boldyrev & Loureiro 2019). In observations, the power along quasi-perpendicular directions are found dominant via the structure function approach (Chen et al. 2010a) and the k-filtering technique (Sahraoui et al. 2010). The wave modes are also anisotropic, as He et al. (2011) and Huang et al. (2020) found that the ion-scale turbulence contains quasi-parallel Alfvén-cyclotron waves (ACWs) and quasi-perpendicular KAWs. The numerical kinetic simulation is another way to explore the physics of anisotropy, and different scalings are reached, for example, $k_\parallel \sim k_\perp$ (Arzamasskiy et al. 2019; Landi et al. 2019), $k_\parallel \sim k_\perp^{1/3}$ (Grošelj et al. 2018) and $k_\parallel \sim k_\perp^{2/3}$ (Cerri et al. 2019).

The previous studies are mainly based on measurements in the vicinity of 1 au. The *Parker Solar Probe (PSP)* spacecraft (Fox et al. 2016), which has reached a perihelion at 0.1 au, could shed light on the physics of nascent solar wind in the inner heliosphere. In this paper, the anisotropy of the magnetic field turbulence at the kinetic scales is investigated, which could be helpful to understand the origin and evolution of the solar wind turbulence in the inner heliosphere. Section 2 describes the data and method used in this work. Section 3 shows the result of the anisotropy. Section 4 is the conclusion and discussion.

2. DATA AND METHOD

The data of the *PSP* at its first perihelion (0.17 au) are used in this study. The FIELDS and Solar Wind Electron Alpha and Proton (SWEAP) instruments provide the *in situ* measurements of the inner-heliospheric solar wind (Bale et al. 2016; Kasper et al. 2016). We use a merged data set from flux-gate magnetometer (FIELDS/MAG) and search coil (FIELDS/SCM) measurements (both operate at 293 Hz), resolving the full range from MHD to kinetic scales simultaneously (Bowen et al. 2020b). The plasma measurements are from the Solar Probe Cup (SWEAP/SPC) (Case et al. 2020). During the perihelion, *PSP* encountered a slow ($V_{SW} < 400$ km/s), but highly Alfvénic solar wind ($\sigma_c \sim 0.7$). The background radial magnetic field is anti-sunward (Bale et al. 2019).

The Morlet wavelet transform is employed to build the PSD of the magnetic fluctuations (Podesta 2009), located at 139 logarithmically spaced frequencies from 0.01 Hz to 149.5 Hz in the spacecraft frame. Part of the inertial range is defined at 0.1 Hz $< f < 1$ Hz, as the ion-scale break frequency is usually larger than 1 Hz at 0.17 au (Duan et al. 2020). The power of the reaction wheels set on the spacecraft contaminates the power spectra around $20 \sim 30$ Hz, so the kinetic range is defined as 30 Hz $< f < 100$ Hz. A short-time-Fourier-transfrom method is used to remove the artificial spikes (Bowen et al. 2020c) (Woodham et al., in preparation). We avoid fitting $f > 100$Hz ranges to avoid SCM noise floor (Bowen et al. 2020b). A piecewise linear fitting in log-log space is implemented to locate the transition range, which is described in Appendix A.

Gaussian windows are used to evaluate the local mean magnetic field directions at different scales, and the angles between the local magnetic field direction and average solar wind velocity direction $\theta_{BV}(f, t)$ are calculated. To estimate the angular distribution of PSD, we partition $\theta_{BV}(f, t)$ into 9 angle bins from $\theta_{BV} \in (90°, 100°]$ to $\theta_{BV} \in (170°, 180°]$. The PSD is averaged over each bins as

$$P(f, \theta_i) = \frac{1}{N_{f,i}} \sum P(f, t)|_{\theta_i < \theta_{BV}(f, t) \le \theta_i + 10°}, \quad (1)$$

where $\theta_i = 10°i + 80°, i = 1, 2, ..., 9$ and $N_{f,i}$ is the numbers of points in each bin at each frequency (Podesta 2009).

3. RESULTS

Figure 1 shows an example interval from 14:30 to 15:30 on Nov 5, 2018. The merged data set is in the Radial-Tangential-Normal (RTN) coordinate system, where B_R is the radial component of the magnetic field along the Sun-spacecraft line. The amplitude of the magnetic field keeps constant as $|B| \sim 90$nT. The average proton density is $\rho_p \sim 316$ cm^{-3}, the solar wind speed is $V_{sw} \sim 344$km/s, and the average proton thermal speed is $w_p \sim 61$ km/s, yielding the Alfvén speed $v_A \sim 109$ km/s, the proton thermal gyroradius $\rho_p \sim 7.1$ km, and the proton inertial length $d_p \sim 13$ km. The plasma β_p is 0.3. The θ_{BR} covers the range from 90° to 180°, allowing to estimate the anisotropy. The inertial, transition and kinetic ranges are observed distinctly in the averaged trace PSD. At the inertial range, the spectral index α_i is -1.56, similar to the statistical result of Chen et al. (2020) at 0.17 au. Then the PSD sharply decreases with $\alpha_t = -3.77$ at the transition range. In the kinetic range, the spectral index increases to $\alpha_k = -2.67$, which is close to -8/3 but larger than -2.8 from studies near 1 au (Alexandrova et al. 2009; Sahraoui et al. 2009). To explore the nature of the transition range, we calculate the normalized reduced magnetic helicity along the radial direction (He et al. 2011; Woodham et al. 2018). Positive helicity represents left-handed (LH) wave modes and negative helicity represent right-handed (RH) modes for sunward background magnetic field. It is revealed that there are two components with opposite polarization around 1 to 20 Hz. The LH modes, locating near 1 to 6 Hz when the magnetic field is quasi-parallel to the radial direction, are identified as coherent ion-scale cyclotron waves (Bowen et al. 2020c). When θ_{BR} is close to 90°, the RH modes dominate around 4 to 20 Hz, which could be the quasi-perpendicular kinetic Alfvénic waves (Huang et al. 2020).

The angular distribution of the PSDs $P(f, \theta_i)$ are shown in Figure 2. From the bottom to top, the different curves correspond to different angular bins from the parallel to the perpendicular directions. The weakest amplitude of the PSD at the parallel direction is larger than the noise level of the SCM, indicating the vadility of the measurement. The PSDs for the remaining angular bins have been offset by 10 for easier viewing. The small bump around 2 Hz in the bottom spectrum is the power of the ion-cycolotron waves along the parallel direction. We demonstrate for the first time that the transition range exist in all of the directions in the inner

heliosphere. The break between the inertial range and the transition range f_{it} is around 2 Hz, and the break between the transition and kinetic ranges f_{tk} is near 6 to Hz. Using Taylor's Hypothesis, we calculate the Doppler frequency corresponding to the scales of ρ_i and d_i in the spacecraft frame. We find that the frequencies of $f_{di} = V_{sw}/2\pi k$ with $kd_i \sim 1$ and $f_{\rho i} = V_{sw}/2\pi k$ with $k\rho_i \sim 1$ are sitting between the spectral break frequencies of f_{it} and f_{tk}. Taylor hypothesis has been shown to hold in the inertial range for the early PSP orbits (Chen et al. 2021). The spectrum with $120° < \theta_{BV} \leq 130°$ is lifted and has more power than the other directions below 20 Hz, which may be enhanced by the reaction wheels of the spacecraft.

Figure 2 (b) shows the spectral anisotropy for the three ranges. The spectral indexes α of each range all have a decreasing trend from the quasi-parallel direction to the quasi-perpendicular direction. The spectral index α_i is -1.4 along the perpendicular direction and $\alpha_i \sim -1.9$ along the parallel direction, demonstrating a similar trend to that of critical-balanced anisotropy observed at 1 au (Horbury et al. 2008; Podesta 2009). In the transition range, the PSD is steepened sharply with $\alpha_t \sim -6.0$ along the parallel direction, and changes to $\alpha_t \sim -3.5$ along the perpendicular direction. This spectral anisotropy has a similar angular dependence with the observation at 1 au (see Figure 4 in Duan et al. (2018)). However, at 1 au, the spectral index varies from around -4 to -2.8, much shallower than the inner heliosphere. Extending to the kinetic scale, the spectral index α_k increase to -2.8 at parallel direction along the parallel direction and -2.6 along the perpendicular direction, which is consistent with the anisotropy of $B_\perp$ spectra from the *Cluster* observation (Chen et al. 2010a).

We define the perpendicular and parallel power spectra as $P_\perp(f) = P(f, 90° < \theta_{BV} \leq 100°)$ and $P_\parallel(f) = P(f, 170° < \theta_{BV} \leq 180°)$. Figure 2 (c) shows the power spectra ratio $(P(f, \theta_{BV})/P_\parallel(f)$, including $P_\perp(f)/P_\parallel(f)$) at three selected frequencies in the three ranges. The power anisotropy $P_\perp/P_\parallel$ is around 4 at 0.5 Hz in the inertial range, and increases to 6 at 4 Hz in the transition range. At the kinetic scale, $P_\perp/P_\parallel$ reaches 20 at 60 Hz, which is much larger than 5 measured by structure function in Chen et al. (2010a). It reveals that below the transition range, the power anisotropy at kinetic scale in the inner heliosphere is stronger than at 1 au.

Using the method introduced by Wang et al. (2020), the structure functions $SF_2(l)$ along the parallel and perpendicular directions are calculated and shown in Figure 3 to explore the wavevector anisotropy, here $l = 1/k$ is the spatial displacement. The spectral indexes α_{SF} of the structure functions are consistent with the in-

dexes α_{PSD} from the PSD as $|\alpha_{SF}| + 1 = |\alpha_{PSD}|$ (Chen et al. 2010a). By equating $SF_2(l_\parallel)$ and $SF_2(l_\perp)$, the anisotropy relation between $l_\parallel$ and $l_\perp$ is estimated. Different ranges manifests different anisotropy. In the transition range (along the perpendicular direction) we get $l_\parallel \sim l_\perp^{0.76}$, which is close to $k_\parallel \sim k_\perp^{2/3}$, the prediction of critical balance (Goldreich & Sridhar 1995) or the intermittent KAW turbulence (Boldyrev & Perez 2012). In principle, l and k have the same anisotropy scaling. Note, however, that ion cyclotron waves in the $k_\parallel$ spectrum may be contributing to this measurement. Below d_i, $l_\parallel \sim l_\perp^{0.37}$ at the kinetic range, similar to the prediction of critical-balance KAW turbulence of $k_\parallel \sim k_\perp^{1/3}$ (Schekochihin et al. 2009).

Statistical analysis of the wavevector anisotropy is performed by dividing the data during 00:00:00 Nov 5-00:00:00 Nov,7 into one-hour intervals with 50% overlapping. The SCM was operating at a 293 Hz sample rate. There are 90 intervals in total. Here we only consider the transition and kinetic ranges, because several directions do not have enough samples (counts < 1000) in the inertial range. Only $\theta_{\rm BV} > 90°$ is considered. Intervals that do not have enough samples in the perpendicular or parallel directions to provide spectra in both directions are also excluded.

Figure 4(a) exhibits the statistical results of the spectral anisotropy. The parallel direction has the steepest indexes, with $\alpha_{t\parallel} = -5.7 \pm 1.3$, and $\alpha_{k\parallel} = -2.9 \pm 0.2$ for the transition and kinetic ranges. The -2.9 index is smaller than the theoretical predictions of -7/3 and -8/3. The spectral indexes of $\alpha_{t\perp} = -3.7 \pm 0.3$ and $\alpha_{k\perp} = -2.57 \pm 0.07$ are observed along the perpendicular direction. This result confirms the existence of a transition range signature in all directions, with a trend that the spectra get steeper from the perpendicular direction to the parallel direction.

Figure 4(b) shows the histograms of the scalings of the wavevector anisotropy. In the transition range along the perpendicular direction, the median scaling is $l_{t\parallel} \sim l_{t\perp}^{0.62 \pm 0.10}$, in line with the prediction of 2/3. The scaling in the kinetic range along the perpendicular direction is 0.37 ± 0.07, following the relation of $l_{k\parallel} \sim l_{k\perp}^{1/3}$.

4. CONCLUSION AND DISCUSSION

In this letter, we present a statistical study of the anisotropy in the kinetic-scale range in the inner heliosphere. By measuring the power spectra along different θ_{BV}, the anisotropy of spectral index and wavevector in the transition range and the kinetic range are investigated. We show that the transition range and the kinetic range have different scalings of anisotropy. The spectral indexes varies from $\alpha_{t\parallel} = -5.7 \pm 1.3$ to $\alpha_{t\perp} =$

-3.7 ± 0.3 in the transition range and $\alpha_{k\parallel} = -2.9 \pm 0.2$ to $\alpha_{k\perp} = -2.57 \pm 0.07$ in the kinetic range. The wavevector anisotropy exhibits the feature of the KAW turbulence, with the scaling of $k_\parallel \sim k_\perp^{0.6}$ in the transition range and changing to $k_\parallel \sim k_\perp^{1/3}$ in the kinetic range.

Similar to the observations at 1 au (Chen et al. 2010a), the anisotropy of the spectral index at 0.17 au shows the trend of the critical balance prediction $k_\perp \gg k_\parallel$, but the substantial difference is the anisotropy in the transition range. The observed transition range could not fit the cascade model of the kinetic waves as -7/3 or -8/3. However, according to the "inertial range - ion dissipation range - electron inertial range" model (Sahraoui et al. 2010), the anisotropy of the spectral index implies the different dissipation mechanisms in the parallel and perpendicular directions. As the KAWs exist along the perpendicular direction (Huang et al. 2020), the perpendicular spectra $P_\perp$ may be interpreted as the Landau damping $P_\perp \sim k^{-4}$ of KAW in transition range (He et al. 2020) and the intermittent KAW cascade model $P_\perp \sim k^{-2.8}$ in the kinetic range (Boldyrev & Perez 2012). Woodham et al. (2021, in prep.) show that the transition range and kinetic range magnetic helicity and magnetic compressibility are also consistent with the transition to KAW turbulence at small scales. For the parallel direction, the -6 spectra is steeper than the prediction of -5 from the critical balance KAW model (Chen et al. 2010b; Schekochihin et al. 2009) and -7/2 from the intermittent KAW model (Boldyrev & Perez 2012). The existence of ion cyclotron waves could explain the extreme steepening by enhancing the power at the onset of the transition range and dissipating significantly to the protons via cyclotron damping (Woodham et al. 2018; He et al. 2019; Bowen et al. 2020c). Below the transition range, the -3 parallel spectra is similar to the simulation of Landi et al. (2019), which proposes a 2D intermittent model at the sub-ion scales. However, the $k_\parallel \sim k_\perp^{1/3}$ anisotropy scaling is inconsistent with the intermittent model.

The ion-scale coherent structures also may contribute the anisotropy. Boldyrev & Loureiro (2019) predicts that the ion-scale current sheets from the tearing instability could mediate the kinetic Alfvénic turbulence to the scalings of $k_\parallel \sim k_\perp^{2/3}$ or $k_\parallel \sim k_\perp$. However, the kinetic tearing instability is predicted to rise significantly around the electron scale, which is difficult to measure with *PSP*.

In addition, the existence of the transition range indicates a strong ion heating in the inner heliosphere. According to Equation (7) from Bowen et al. (2020a), the heating ratio from the cascade energy flux at the transition range could be estimated under the assumption

of the Batchelor cascade model. The heating ratio from the parallel spectrum ($> 99\%$) is stronger than the perpendicular spectrum ($\sim 90\%$), which is consistent with the power anisotropy at the kinetic scale. How the field energy transfers to the particles quantitatively along different directions needs a further study combining field and particle measurements.

APPENDIX

A. PIECEWISE PSD FITTING FOR TRANSITION RANGES

To determine the frequency range of the transition range, we divide the PSD(f) into three sections, which connect one another at the points of f_1 and f_2, respectively. The inertial range is from 0.1 Hz to f_1, the transition range is from f_1 to f_2, and the kinetic range is from f_2 to 100 Hz. We implement linear fitting to each range and get a piecewise linear fitting function in the log-log space:

$$\log_{10} \mathrm{PSD}_{fit}(f; f_1, f_2) = \begin{cases} \alpha_i \log_{10} f + b_i & 0.1 \text{ Hz} < f \leq f_1 \\ \alpha_t \log_{10} f + b_t & f_1 < f \leq f_2 \\ \alpha_k \log_{10} f + b_k & f_2 < f \leq 100 \text{ Hz} \end{cases} \tag{A1}$$

Then we compute the deviation function:

$$\mathrm{Dev}(f_1, f_2) = \sum_{i=1}^{n} [\log_{10} \mathrm{PSD}_{fit}(f_i; f_1, f_2) - \log_{10} \mathrm{PSD}(f_i)]^2,$$

n is the total number of the frequencies. We search the best f_1 and f_2 to minimize the deviation function and finally we get the frequency range $[f_1, f_2]$ as the transition range.

ACKNOWLEDGMENTS

REFERENCES

Alexandrova, O., Lacombe, C., Mangeney, A., Grappin, R., & Maksimovic, M. 2012, ApJ, 760, 121, doi: 10.1088/0004-637X/760/2/121

Alexandrova, O., Saur, J., Lacombe, C., et al. 2009, PhRvL, 103, 165003

Arzamasskiy, L., Kunz, M. W., Chandran, B. D. G., & Quataert, E. 2019, The Astrophysical Journal, 879, 53, doi: 10.3847/1538-4357/ab20cc

Bale, S. D., Kellogg, P. J., Mozer, F. S., Horbury, T. S., & Reme, H. 2005, Physical Review Letters, 94, 215002, doi: 10.1103/PhysRevLett.94.215002

Bale, S. D., Goetz, K., Harvey, P. R., et al. 2016, Space Science Reviews, 204, 49, doi: 10.1007/s11214-016-0244-5

Bale, S. D., Badman, S. T., Bonnell, J. W., et al. 2019, Nature, 576, 237, doi: 10.1038/s41586-019-1818-7

Boldyrev, S. 2006, Physical Review Letters, 96, 1, doi: 10.1103/PhysRevLett.96.115002

Boldyrev, S., & Loureiro, N. F. 2019, Phys. Rev. Research, 1, 012006, doi: 10.1103/PhysRevResearch.1.012006

Boldyrev, S., & Perez, J. C. 2012, The Astrophysical Journal, 758, L44, doi: 10.1088/2041-8205/758/2/l44

Bowen, T. A., Mallet, A., Bale, S. D., et al. 2020a, Physical review letters, 125, 025102
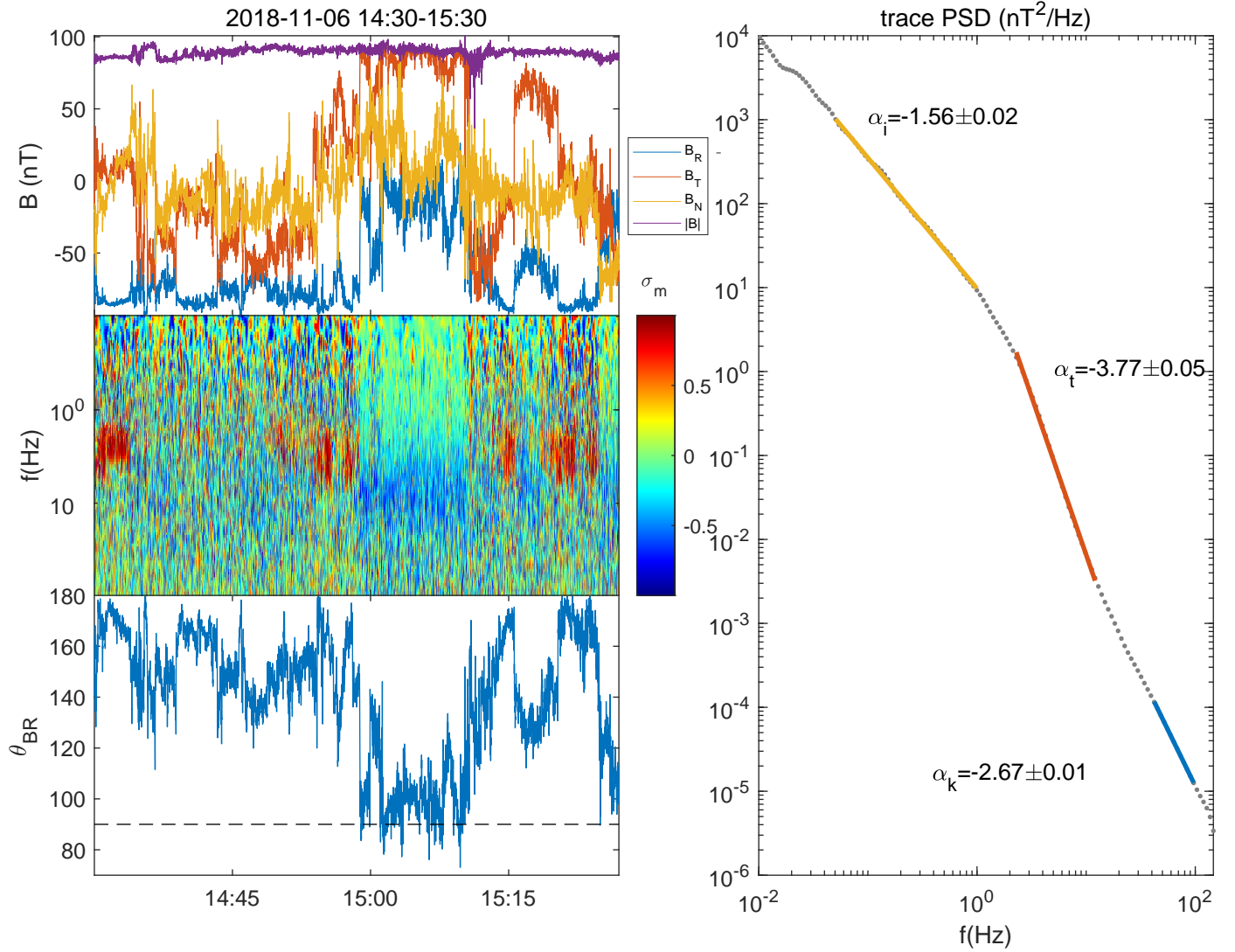
Figure 1. The overview of the interval from 14:30 to 15:30 on Nov 6, 2018. (a) The magnetic field in the RTN coordinates. (b) The reduced magnetic helicity σ_m along the radial direction. Positive values indicate LH modes and negative values indicate RH modes. (c) The angle between the magnetic field and the radial direction θ_{BR}. (d) The averaged trace PSD (grey dots) over the interval. The dash lines are the linear fittings to inertial (yellow), transition (red) and kinetic (blue) ranges.

Bowen, T. A., Bale, S. D., Bonnell, J. W., et al. 2020b,
    Journal of Geophysical Research: Space Physics, 125,
    e2020JA027813, doi: 10.1029/2020JA027813

Bowen, T. A., Mallet, A., Huang, J., et al. 2020c, The
    Astrophysical Journal Supplement Series, 246, 66,
    doi: 10.3847/1538-4365/ab6c65

Bruno, R., & Carbone, V. 2013, Living Reviews in Solar
    Physics, 10, doi: 10.12942/lrsp-2013-2

Case, A. W., Kasper, J. C., Stevens, M. L., et al. 2020, The
    Astrophysical Journal Supplement Series, 246, 43,
    doi: 10.3847/1538-4365/ab5a7b

Cerri, S. S., GroÅ¡elj, D., & Franci, L. 2019, Frontiers in
    Astronomy and Space Sciences, 6, 64,
    doi: 10.3389/fspas.2019.00064

Chen, C. H., Horbury, T. S., Schekochihin, A. A., et al.
    2010a, Physical Review Letters, 104, 1,
    doi: 10.1103/PhysRevLett.104.255002

Chen, C. H. K., Bale, S. D., Salem, C. S., & Maruca, B. A.
    2013, ApJ, 770, 125, doi: 10.1088/0004-637X/770/2/125

Chen, C. H. K., & Boldyrev, S. 2017, ApJ, 842, 122,
    doi: 10.3847/1538-4357/aa74e0

Chen, C. H. K., Klein, K. G., & Howes, G. G. 2019, Nature
    Communications, 10, 740,
    doi: 10.1038/s41467-019-08435-3
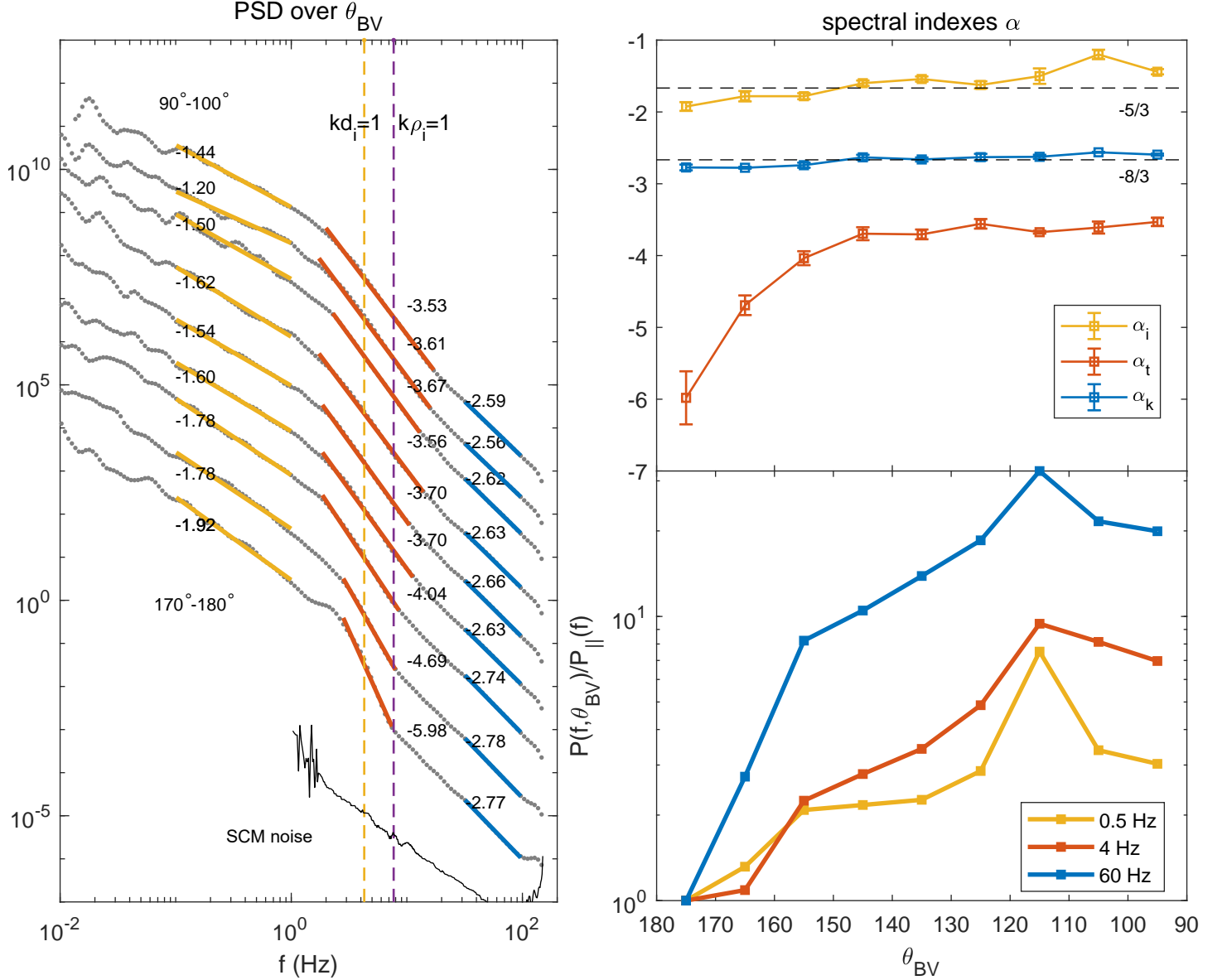
Figure 2. (a) The magnetic PSDs in different angle bins. The colored dashed lines are the fitted inertial (yellow), transition (red) and kinetic (blue) ranges. Black spectrum is the noise level of the SCM. The spectral indexes are also shown. The vertical dashed lines indicate the characteristic scales d_i (yellow) and ρ_i (purple). (b) Spectral indexes of the three ranges estimated from different θ_{BV} bins. (c) The power anisotropy at three specific frequencies respectively located in the inertial (0.5 Hz, yellow), transition (4Hz, red) and kinetic (60 Hz, blue) ranges over different θ_i.

Chen, C. H. K., Wicks, R. T., Horbury, T. S., & Schekochihin, A. A. 2010b, ApJ, 711, L79, doi: 10.1088/2041-8205/711/2/L79

Chen, C. H. K., Bale, S. D., Bonnell, J. W., et al. 2020, ApJS, 246, 53, doi: 10.3847/1538-4365/ab60a3

Chen, C. H. K., Chandran, B. D. G., Woodham, L. D., et al. 2021, arXiv e-prints, arXiv:2101.00246. https://arxiv.org/abs/2101.00246

Duan, D., He, J., Pei, Z., et al. 2018, ApJ, 865, 89, doi: 10.3847/1538-4357/aad9aa

Duan, D., Bowen, T. A., Chen, C. H. K., et al. 2020, The Astrophysical Journal Supplement Series, 246, 55, doi: 10.3847/1538-4365/ab672d

Fox, N. J., Velli, M. C., Bale, S. D., et al. 2016, Space Science Reviews, 204, 7, doi: 10.1007/s11214-015-0211-6

Goldreich, P., & Sridhar, S. 1995, ApJ, 438, 763, doi: 10.1086/175121
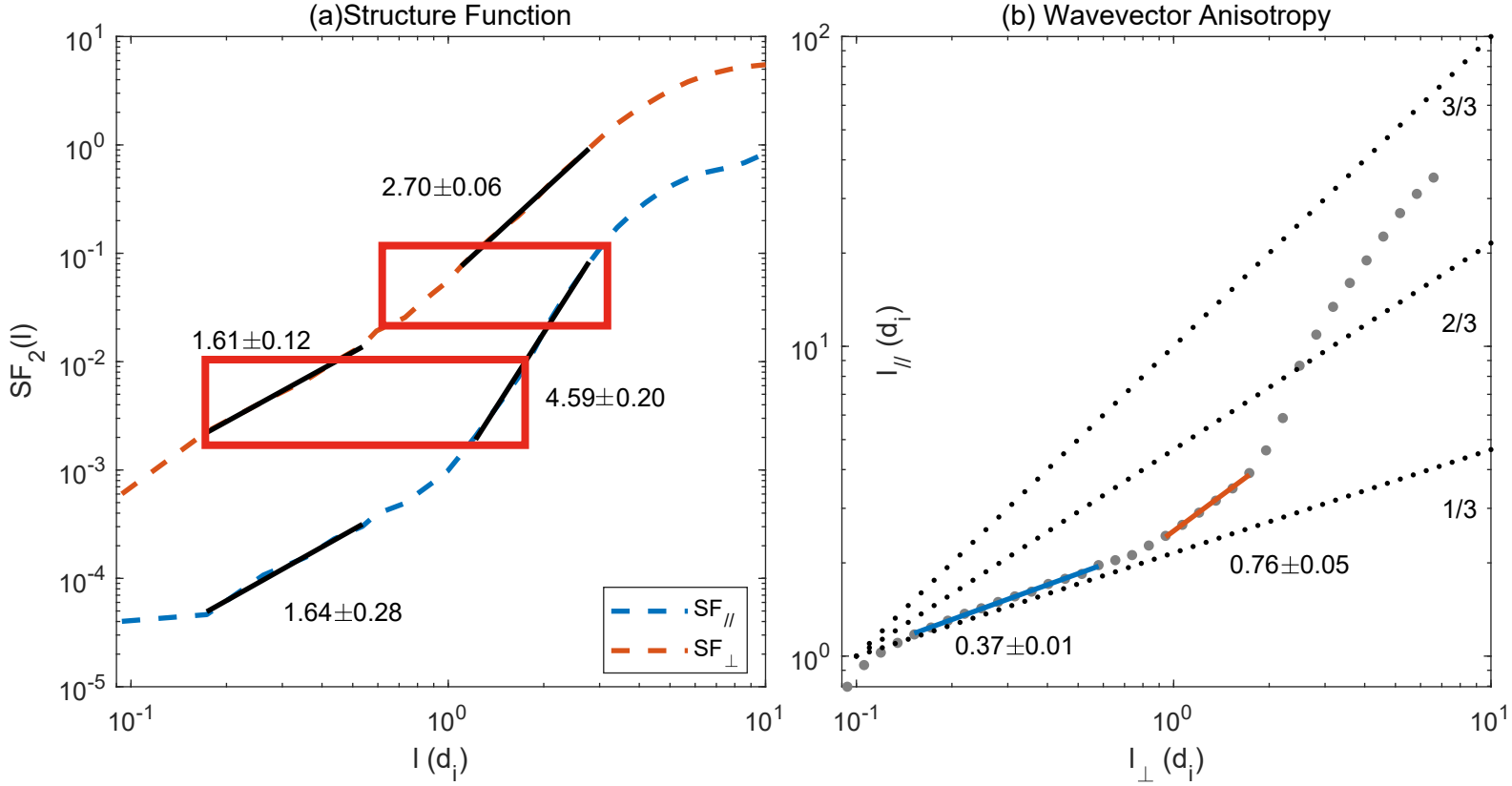
Figure 3. (a) Structure functions along the parallel (blue) and perpendicular (red) directions. Black lines are the fitting results in both the transition and kinetic ranges. Red squares indicate the equal values of the SF_2. (b) Wavevector anisotropy derived from (a). Blue and red lines are for the kinetic and transition ranges (along the perpendicular direction), respectively. Three typical relations are presented as black dot lines for reference.

Grošelj, D., Mallet, A., Loureiro, N. F., & Jenko, F. 2018, Physical Review Letters, 120, 1, doi: 10.1103/PhysRevLett.120.105101

He, J., Marsch, E., Tu, C., Yao, S., & Tian, H. 2011, ApJ, 731, 85, doi: 10.1088/0004-637X/731/2/85

He, J., Tu, C., Marsch, E., Bourouaine, S., & Pei, Z. 2013, ApJ, 773, 72, doi: 10.1088/0004-637X/773/1/72

He, J., Zhu, X., Verscharen, D., et al. 2020, The Astrophysical Journal, 898, 43

He, J., Duan, D., Wang, T., et al. 2019, The Astrophysical Journal, 880, 121

Horbury, T. S., Forman, M., & Oughton, S. 2008, Physical Review Letters, 101, 175005, doi: 10.1103/PhysRevLett.101.175005

Howes, G. G., Cowley, S. C., Dorland, W., et al. 2008, Journal of Geophysical Research: Space Physics, 113, 1, doi: 10.1029/2007JA012665

Huang, S., Zhang, J., Sahraoui, F., et al. 2020, arXiv preprint arXiv:2006.04665

Kasper, J. C., Abiad, R., Austin, G., et al. 2016, Space Science Reviews, 204, 131

Landi, S., Franci, L., Papini, E., et al. 2019, Spectral anisotropies and intermittency of plasma turbulence at ion kinetic scales. https://arxiv.org/abs/1904.03903

Lion, S., Alexandrova, O., & Zaslavsky, A. 2016, ApJ, 824, 47, doi: 10.3847/0004-637x/824/1/47

Mallet, A., Schekochihin, A. A., & Chandran, B. D. G. 2017, Journal of Plasma Physics, 83, 905830609, doi: 10.1017/S0022377817000812

Meyrand, R., Squire, J., Schekochihin, A. A., & Dorland, W. 2020, arXiv e-prints, arXiv:2009.02828. https://arxiv.org/abs/2009.02828

Podesta, J. J. 2009, ApJ, 698, 986, doi: 10.1088/0004-637X/698/2/986

Sahraoui, F., Goldstein, M. L., Belmont, G., Canu, P., & Rezeau, L. 2010, Physical Review Letters, 105, 131101, doi: 10.1103/PhysRevLett.105.131101

Sahraoui, F., Goldstein, M. L., Robert, P., & Khotyaintsev, Y. V. 2009, Physical Review Letters, 102, 231102, doi: 10.1103/PhysRevLett.102.231102

Saito, S., Gary, S. P., Li, H., & Narita, Y. 2008, Physics of Plasma, 15, 102305
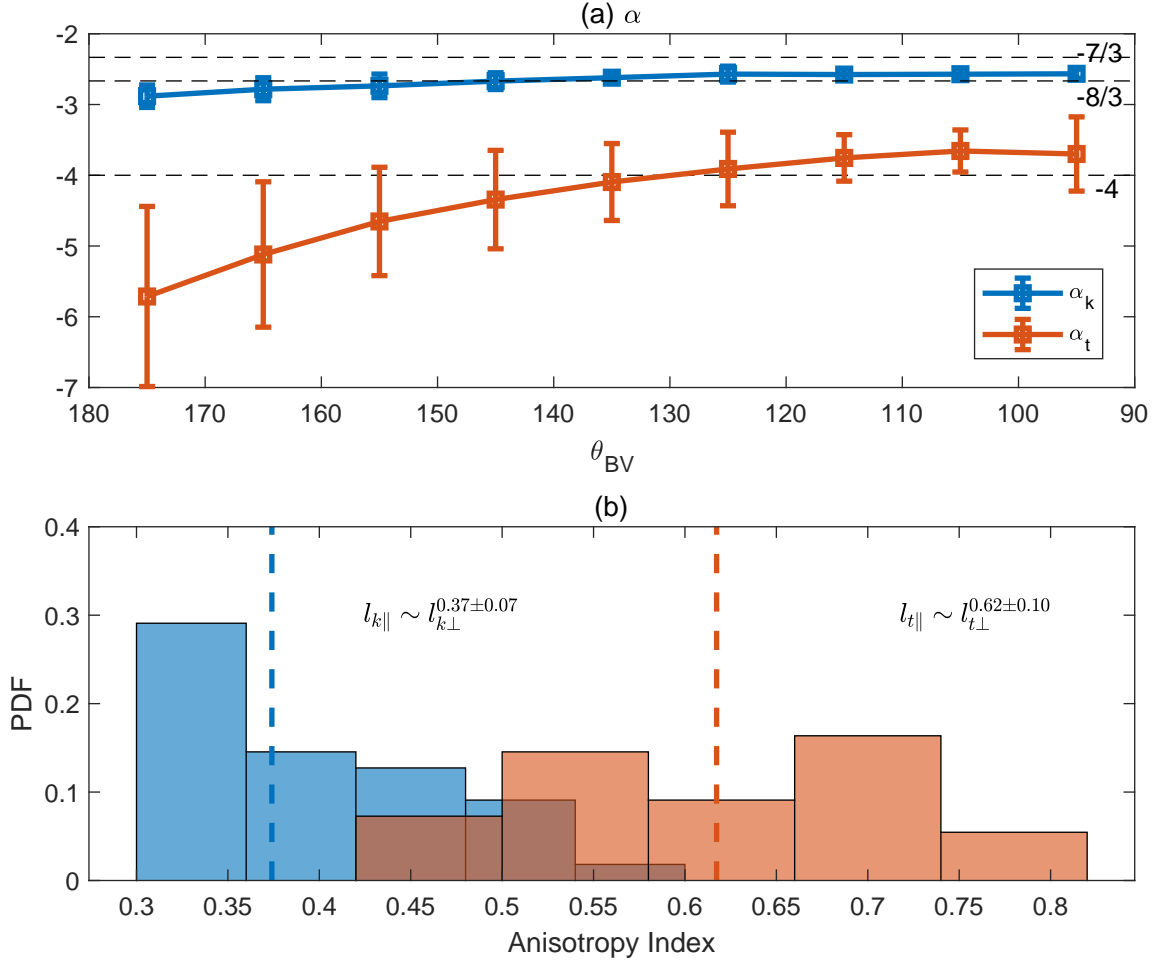
Figure 4. (a) The statistical result of the spectral anisotropy. (b) The statistical result of the wavevector anisotropy. Red indicates the transition range and blue indicates the kinetic range. Dashed lines are the medians of the indexes.

Schekochihin, A. A., Cowley, S. C., Dorland, W., et al. 2009, The Astrophysical Journal Supplement Series, 182, 310, doi: 10.1088/0067-0049/182/1/310

Verdini, A., Grappin, R., Alexandrova, O., et al. 2019, Monthly Notices of the Royal Astronomical Society, 486, 3006, doi: 10.1093/mnras/stz1041

Voitenko, Y., & Keyser, J. D. 2016, ApJL, 832, L20, doi: 10.3847/2041-8205/832/2/l20

Wang, T., He, J., Alexandrova, O., Dunlop, M., & Perrone, D. 2020, ApJ, 898, 91

Wang, X., Tu, C., He, J., Marsch, E., & Wang, L. 2014, ApJ, 783, L9, doi: 10.1088/2041-8205/783/1/L9

Woodham, L. D., Wicks, R. T., Verscharen, D., & Owen, C. J. 2018, ApJ, 856, 49, doi: 10.3847/1538-4357/aab03d

Wu, H., Tu, C., Wang, X., et al. 2020, The Astrophysical Journal, 892, 138, doi: 10.3847/1538-4357/ab7b72

Zhao, J., Voitenko, Y., Wu, D., & Yu, M. 2016, Journal of Geophysical Research: Space Physics, 121, 5